# Supporting Information

## Experimental and theoretical investigations on Se(IV) and Se(VI) adsorption to UiO-66-based metal-organic frameworks

Jingmiao Wei [a], Wei Zhang [b], Weiyi Pan [c], Chaoran Li [d] and Weiling Sun *[a]

[a] College of Environmental Sciences and Engineering, Peking University, The Key Laboratory of Water and Sediment Sciences, Ministry of Education, Beijing 100871, China

[b] Department of Plant, Soil and Microbial Sciences; Environmental Science, and Policy Program, Michigan State University, East Lansing, Michigan 48824, United States

[c] Shenzhen Key Laboratory for Heavy Metal Pollution Control and Reutilization, School of Environment and Energy, Peking University Shenzhen Graduate School, Shenzhen 518055, China

[d] College of Life and Environmental Sciences, Minzu University of China, Beijing 100081, China

**Preparation of adsorbents**

To synthesize UiO-66, 0.204 g of 1,4-benzenedicarboxylic acid ($H_2BDC$) was dissolved in 9.4 mL N,N-dimethylformamide (DMF) under vigorous stirring. After 15 minutes, 2.3 mL of $CH_3COOH$ was added dropwise to the solution at a rate of ~1 drop per second to accelerate the formation of crystals. Then, 0.318 g $ZrCl_4$ was dissolved in 9.4 mL DMF under vigorous stirring for 30 minutes.[1] Afterwards, the two solutions were mixed in a beaker and vigorously stirred for another 20 minutes. The obtained mixture was sealed into a Teflon-lined autoclave and maintained in a pre-heated oven at 120 °C for 24 h. After cooling to room temperature, the obtained crystals were centrifugalized at 5000 rpm for 30 min and immersed in 100 mL of ethanol for 5 days. The ethanol was replaced 3 times per day. After that, the crystals were separated from the ethanol by centrifuging at 5000 rpm for 30 min. Finally, the synthesized material was freeze-dried at −60 °C for 3 h in vacuum. To synthesize UiO-66-$NH_2$, the same method was used, but $NH_2$-BDC (0.2466 g) was used in place of $H_2BDC$.[2]

**Data analysis**

**Adsorption kinetics**

The adsorption amount of Se(IV) or Se(VI), $Q_e$ (mg/g), was calculated as follows:[3]

$$Q_e = \frac{C_0 - C_e}{m} \quad \text{(S1)}$$

where $C_0$ (mg/L) and $C_e$ (mg/L) are the initial and final concentrations of Se, respectively. $m$ (g/L) is the dosage of MOFs.

The experimental data were described by the widely used pseudo-first order and pseudo-

second order models, as shown in Eq. (S2) and (S3), respectively.[4-6]

$$q_{\mathrm{t}} = q_{\mathrm{e}}(1 - \frac{1}{e^{k_1 t}}) \tag{S2}$$

$$q_{\mathrm{t}} = \frac{t}{\frac{1}{k_2 q_{\mathrm{e}}^2} + \frac{t}{q_{\mathrm{e}}}} \tag{S3}$$

where $q_{\mathrm{t}}$ is the amount of Se adsorbed at time $t$ (mg/g), $q_{\mathrm{e}}$ is the equilibrium adsorption amount (mg/g), $k_1$ is the pseudo-first order rate constant (1/min), and $k_2$ is the pseudo-second order rate constant (g/(mg·min)).

The intra-particle diffusion model in Eq. (S4) was used to determine whether intraparticle diffusion was the rate-limiting step:[7]

$$q_{\mathrm{t}} = k_{\mathrm{p}} t^{0.5} + C \tag{S4}$$

where $k_{\mathrm{p}}$ is the intraparticle diffusion rate constant (mg/(g·min$^{0.5}$)), $C$ is the instaneous adsorption amount on the external surface and a constant related to the boundary layer thickness. If the rate-limiting step is the intra-particle diffusion, the plot of $q_{\mathrm{t}}$ against the square root of time should be a straight line and pass through the origin ($C$ = 0). Otherwise, the deviation of the plot from the linearity indicates the rate-limiting step should be the boundary layer (film) diffusion.

The Elovich model in Eq. (S5) was used to describe the kinetic experiments:[8]

$$\frac{\mathrm{d}q_t}{dt} = a \exp(-bq_t) \tag{S5}$$

where $a$ is the initial adsorption rate (mg/g min), $b$ is a constant related to the surface coverage (g/mg). When $q_t \rightarrow 0$, $\mathrm{d}q_t/\mathrm{d}t \rightarrow$ a, given that $q_t = 0$ at $t = 0$, if $t$ ? $t_0$, the equation S5 becomes S6:

$$a\,q_t = \frac{1}{b}\ln(ab) + \frac{1}{b}\ln t \tag{S6}$$

the equation S6 can be simplified to S7:

$$q_t = A + 2.303B\log t \tag{S7}$$

where $A$ and $B$ are two constants represent $\frac{1}{b}\ln(ab)$ and $\frac{1}{b}$, respectively.

**Adsorption isotherm**

Adsorption isotherms were fitted using the Langmuir and Freundlich models.[9]

$$Q_e = Q_{max}\frac{K_L C_e}{1 + K_L C_e} \tag{S8}$$

where $Q_{max}$ (mg/g) is the adsorption capacity and $K_L$ (L/mg) is the Langmuir adsorption affinity parameter.

$R_L$ is a constant to describe the adsorption in Langmuir model.[9]

$$R_L = \frac{1}{1 + K_L C_0} \tag{S9}$$

Freundlich models[8]:

$$Q_e = Q_{max}\frac{K_L C_e}{1 + K_L C_e} \tag{S10}$$

where $K_F$ (mg/g (mg/L)$^{-1/n}$) is the Freundlich distribution coefficient, and 1/n is the empirical Freundlich constant describing the adsorption intensity or surface heterogeneity.[9]

68 **Table S1** The XPS Elemental Analysis of the MOFs

| Sample | C (%) | O (%) | Zr (%) | N (%) | Se (%) |
|---|---|---|---|---|---|
| UiO-66 | 59.61 | 35.63 | 4.76 | -- | -- |
| UiO-66-$NH_2$ | 57.89 | 33.14 | 3.98 | 4.99 | -- |
| Se(IV)-adsorbed UiO-66 | 51.09 | 40.91 | 5.19 | -- | 2.81 |
| Se(VI)-adsorbed UiO-66 | 54.89 | 40.61 | 4.19 | -- | 0.31 |
| Se(IV)-adsorbed UiO-66-$NH_2$ | 52.00 | 35.84 | 4.43 | 5.53 | 2.20 |
| Se(VI)-adsorbed UiO-66-$NH_2$ | 57.89 | 32.95 | 3.92 | 5.00 | 0.24 |

69

**Table S2** The XPS Peak Composition Analysis of the MOFs

| | C 1s (%) | | | | O 1s (%) | | | Zr 3d (%) | | N 1s (%) | |
|---|---|---|---|---|---|---|---|---|---|---|---|
| | C-C/C=C 284.8 eV | C-N 284.9 eV | C-O 286.2 eV | –COO 288.7 eV | O-Zr 530.2 eV | O=C 531.8 eV | O-C 533.1 eV | Zr 3d5/2 182.7 eV | Zr 3d3/2 185.1 eV | Ph $NH_2$ N 399.2 eV | Ph $NH_3^+$ N 400.4 eV |
| UiO-66 | 68.37 | -- | 11.15 | 20.49 | 16.13 | 77.09 | 6.78 | 61.09 | 38.91 | | |
| UiO-66-$NH_2$ | 46.20 | 5.98 | 22.15 | 25.67 | 11.89 | 76.55 | 11.56 | 60.59 | 39.41 | 31.40 | 68.60 |
| Se(IV)-adsorbed UiO-66 | 68.43 | -- | 10.90 | 20.67 | 12.37 | 73.43 | 14.20 | 53.93 | 46.07 | | |
| Se(VI)-adsorbed UiO-66 | 74.55 | -- | 7.06 | 18.39 | 10.99 | 63.17 | 25.83 | 62.37 | 37.63 | | |
| Se(IV)-adsorbed UiO-66-$NH_2$ | 59.40 | -- | 19.35 | 21.26 | 12.32 | 73.63 | 14.05 | 54.58 | 45.42 | 44.74 | 55.26 |
| Se(VI)-adsorbed UiO-66-$NH_2$ | 61.51 | -- | 17.63 | 20.86 | 13.29 | 68.16 | 18.54 | 60.57 | 39.43 | 46.83 | 53.17 |

**Table S3** Kinetic Parameters for Se(IV) and Se(VI) Adsorption by MOFs

| Sorbates | Sorbents | $q_{e,exp}$[a] | Pseudo-first-order | | | Pseudo-second-order | | | Intra-particle | | | Elovich model | | |
|---|---|---|---|---|---|---|---|---|---|---|---|---|---|---|
| | | | $q_e$ | $k_1$[b] | $R^2$ | $q_e$ | $k_2$[c] | $R^2$ | $k_p$ | C | $R^2$ | A | B | $R^2$ |
| Se(IV) | UiO-66 | 29.1 | 3.51 | 0.0033 | 0.629 | 28.0 | 0.0325 | 0.901 | 0.253 | 23.4 | 0.592 | 20.4 | 1.43 | 0.878 |
| | UiO-66-$NH_2$ | 25.7 | 2.03 | 0.0020 | 0.223 | 25.1 | 0.0354 | 0.977 | 0.197 | 21.2 | 0.445 | 18.5 | 1.20 | 0.775 |
| Se(VI) | UiO-66 | 5.88 | 0.597 | 0.0036 | 0.360 | 5.84 | 0.0555 | 0.999 | 0.042 | 4.93 | 0.454 | 4.93 | 0.0180 | 0.454 |
| | UiO-66-$NH_2$ | 3.16 | 0.687 | 0.0014 | 0.298 | 3.08 | 0.0472 | 0.996 | 0.013 | 2.70 | 0.523 | 2.70 | 0.00560 | 0.523 |

[a] mg/g, [b] 1/min, [c] g/(mg·min), and [d] mg/(g·$min^{0.5}$)

**Table S4** Parameters of the Isotherm Models for Se(IV) and Se(VI) adsorption by MOFs

| | Sorbates | Sorbents | Langmuir | | | | Freundlich | | |
|---|---|---|---|---|---|---|---|---|---|
| | | | $Q_{max}$[a] | $k_L$[b] | $R^2$ | $R_L$ | $K_F$[c] | 1/n | $R^2$ |
| Original | Se(IV) | UiO-66 | 59.9 | 0.223 | 0.961 | 0.0360-0.473 | 13.1 | 0.395 | 0.908 |
| | | UiO-66-$NH_2$ | 26.8 | 0.356 | 0.993 | 0.0229-0.360 | 7.38 | 0.352 | 0.962 |
| | Se(VI) | UiO-66 | 37.3 | 0.0299 | 0.938 | 0.218-0.870 | 1.50 | 0.690 | 0.986 |
| | | UiO-66-$NH_2$ | 11.9 | 0.103 | 0.994 | 0.0749-0.660 | 1.63 | 0.471 | 0.954 |
| BET surface area normalized | Se(IV) | UiO-66 | 0.0426 | 0.404 | 0.941 | -- | 0.0142 | 0.306 | 0.955 |
| | | UiO-66-$NH_2$ | 0.0399 | 0.358 | 0.960 | -- | 0.0140 | 0.269 | 0.962 |
| | Se(VI) | UiO-66 | 0.0364 | 0.0247 | 0.984 | -- | 0.0020 | 0.560 | 0.963 |
| | | UiO-66-$NH_2$ | 0.0186 | 0.0913 | 0.981 | -- | 0.0038 | 0.350 | 0.939 |

[a] mg/g, [b] L/mg, and [c] mg/g $(mg/L)^{-1/n}$

**Table S5** Comparison of Se(IV) and Se(VI) Adsorption Capacity for Various Adsorbents

| Adsorbents | Adsorbates | Adsorption capacity (mg/g) | Initial concentration of Se (mg/L) | Adsorbent concentration (g/L) | pH |
|---|---|---|---|---|---|
| $CuFe_2O_4$[9] | Se(IV & VI) | 14.1 & 5.97 | 1-25 | 0.4 | 7.4 |
| Coal fly ash/cement composite[11] | Se(IV & VI) | 15.8 & 38.8 | 3.95-118.5 | 20 | 11 |
| $MnFe_2O_4$NM[12] | Se(IV & VI) | 6.6 & 0.8 | 0.25-10 | 2.5 | 4 |
| Magnetic nanoparticle–graphene oxide composites[13] | Se(IV & VI) | 23.8 & 15.1 | 0.05-500 | 1 | 6-9 |
| n-$Al_2O_3$ impregnated chitosan beads[14] | Se(IV & VI) | 11.08 &20.11 | 1 | 1.75 | 6.7-6.8 |
| Eggshell membranes[15] | Se | 0.16 | 0.8 | 5 | 8.5 |
| Chitosan–montmorillonite composite[16] | Se(IV & VI) | 18.4 | 0.11-10 | 0.5 | 4-7 |
| MBHB incorporated into mesoporous silica[17] | Se(IV) | 93.56 | 2.02-74.16 | 1.0 | 1.5 |
| DSDH incorporated into mesoporous silica[18] | Se(IV) | 111.12 | 1.02-70.24 | 0.5 | 2.0 |
| HMBA incorporated into mesoporous inorganic silica[19] | Se(IV) | 103.73 | 1-80 | 0.5 | 2.5 |
| Nano-magnetite[20] | Se(IV & VI) | 6 | 0.1-5 | 0.1 | 4 |
| $Fe_3O_4$ nanomaterials[21] | Se(IV & VI) | 2.38 & 2.37 | 0.25-10 | 2.5 | 4 |
| Nano $TiO_2$ colloid[22] | Se(IV) | 27.1 | 0.1-1.5 | 2 | 6-7 |
| Mg–Al–$CO_3$ layered double hydroxide[23] | Se(IV & VI) | 160 & 90 | 5-500 | 2 | 5 |
| Mg–Fe–$CO_3$ layered double hydroxide[24] | Se(IV) | 32.05 | 30-70 | 1 | 6 |
| nα-$Fe_2O_3$ synthesized from $FeCl_3$[25] | Se(IV & VI) | 40.2 &15.6 | --- | 0.005 | 5.5-6.6 |
| Fe–Mn hydrous oxides[26] | Se(IV & VI) | 41.02 & 19.84 | 5-500 | 2 | 4 |
| Nano-$TiO_2$[27] | Se(IV) | 8.46 | 10-54 | 5 | 5 |
| NU-1000[28] | Se(IV & VI) | 95&85 | 100 | 2 | 6 |
| UiO-66-HCl[29] | Se(VI) | 86.8 | 150 | 1 | 6.8 |
| Uncultivated soils under Cerrado biome[30] | Se(VI) | 0.008 | 0-2 | 100 | 5.5 |
| UiO-66 | Se(IV & VI) | 59.9 & 37.3 | 5-120 | 0.5 | 6 |
| UiO-66-$NH_2$ | Se(IV & VI) | 26.8 & 11.9 | 5-120 | 0.5 | 6 |

**Table S6** Binding Energy of Se(IV) Adsorbed on UiO-66 and UiO-66-$NH_2$

| Species | E (Hartree) | Adsorption sites | | E (Hartree) | Binding energy (kJ/mol) | Bond length/Distance (Å) |
|---|---|---|---|---|---|---|
| UiO-66 | -6842.00 | | | | | |
| $SeO_3^{2-}$ | -597.76 | A | 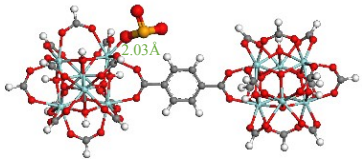  Zr—O⁻-Se(O⁻)=O | -7439.81 | -135.45 | 2.03 |
| | | C | 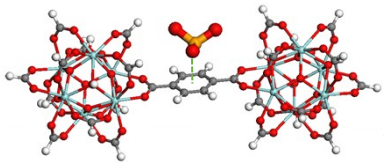 benzene—O=Se(O⁻)-O⁻ | -7439.77 | -27.36 | -- |
| | | D | 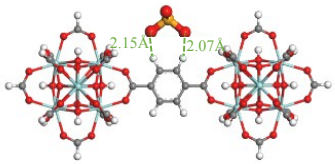  benzene-H—O⁻-Se(O⁻)=O | -7439.78 | -70.83 | 2.15/2.07 |
| $HSeO_3^-$ | -598.26 | A | 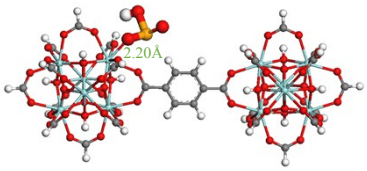  Zr—O⁻-Se(OH)=O | -7440.28 | -59.36 | 2.20 |
| | | B | 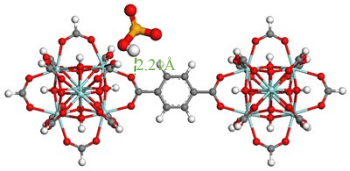  Zr-O—HO-Se(O⁻)=O | -7440.27 | -48.84 | 2.21 |
| | | C | 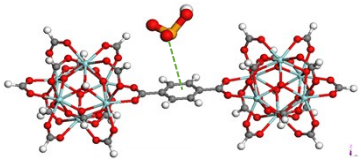 benzene—O=Se(OH)-O⁻ | -7440.27 | -26.40 | -- |
| | | D | 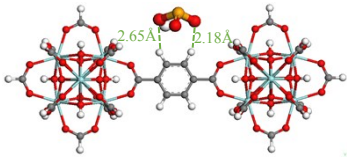  benzene-H—O⁻-Se(OH)=O | -7440.27 | -34.97 | 2.65/2.18 |

| Species | E (Hartree) | Adsorption sites | | E (Hartree) | Binding energy (kJ/mol) | Bond length/Distance (Å) |
|---|---|---|---|---|---|---|
| $H_2SeO_3$ | -598.71 | A | 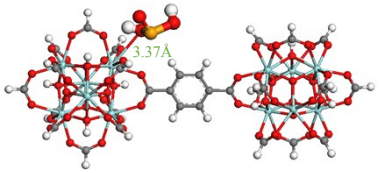  Zr—OH-Se(OH)=O | -7440.72 | -11.36 | 3.37 |
| | | B | 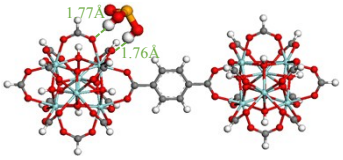  Zr-O—HO-Se(OH)=O | -7440.72 | -29.79 | 1.77/1.76 |
| | | C | 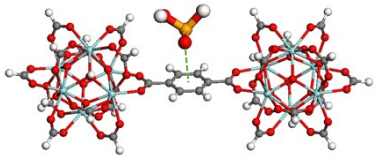 benzene—O=Se(OH)-OH | -7440.71 | -4.96 | -- |
| | | D | 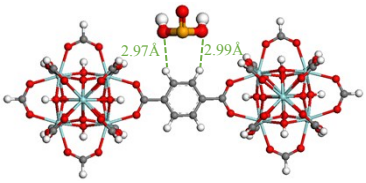  benzene-H—OH-Se(OH)=O | -7440.71 | -2.93 | 2.97/2.99 |
| $SeO_4^{2-}$ | -673.00 | A | 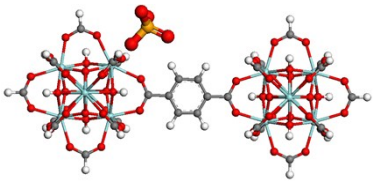 | -7515.01 | -50.58 | 2.10 |
| UiO-66-$NH_2$ | -6897.37 | | | | | |
| $SeO_3^{2-}$ | -597.76 | A | 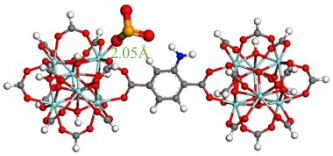  Zr—O⁻-Se(O⁻)=O | -7495.19 | -141.89 | 2.05 |
| | | C | 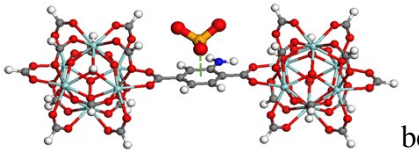 benzene—O=Se(O⁻)-O⁻ | -7495.14 | -13.12 | -- |

| Species | E (Hartree) | Adsorption sites | | E (Hartree) | Binding energy (kJ/mol) | Bond length/Distance (Å) |
|---|---|---|---|---|---|---|
| | | D | 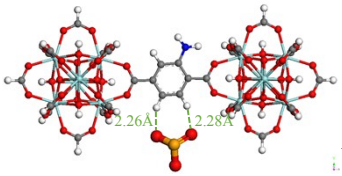 benzene-H—O⁻-Se(O⁻)=O | -7495.16 | -67.61 | 2.26/2.28 |
| | | E | 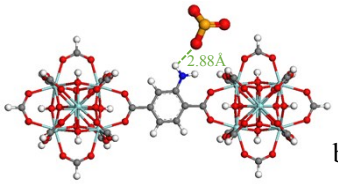 benzene-N(H)-H—O⁻-Se(O⁻)=O | -7495.15 | -57.50 | 2.88 |
| $HSeO_3^-$ | -598.26 | A | 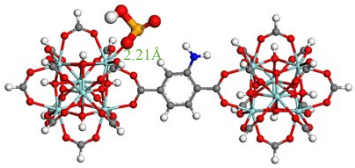 Zr—O⁻-Se(OH)=O | -7495.66 | -70.60 | 2.21 |
| | | B | 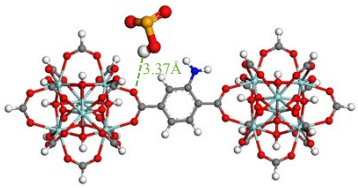 Zr-O—HO-Se(O⁻)=O | -7495.65 | -39.54 | 3.37 |
| | | C | 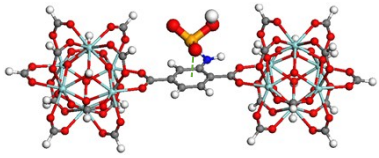 benzene—O=Se(OH)-O⁻ | -7495.64 | -28.61 | -- |
| | | D | 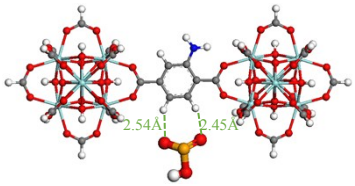 benzene-H—O⁻-Se(OH)=O | -7495.65 | -36.52 | 2.54/2.45 |
| | | E | 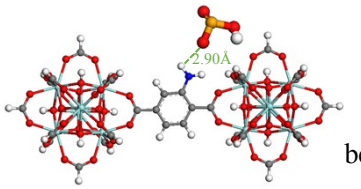 benzene-N(H)-H—O⁻-Se(OH)=O | -7495.65 | -47.63 | 2.90 |

| Species | E (Hartree) | Adsorption sites | | E (Hartree) | Binding energy (kJ/mol) | Bond length/Distance (Å) |
|---|---|---|---|---|---|---|
| $H_2SeO_3$ | -598.71 | A | 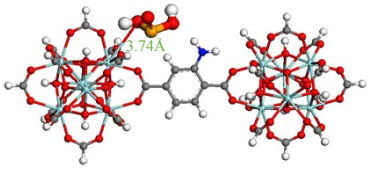  Zr—OH-Se(OH)=O | -7496.09 | -20.00 | 3.74 |
| | | B | 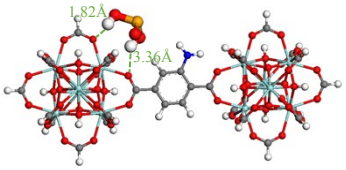  Zr-O—HO-Se(OH)=O | -7496.09 | -24.38 | 1.82/3.36 |
| | | C | 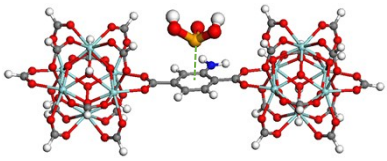 benzene—O=Se(OH)-OH | -7496.09 | -5.32 | -- |
| | | D | 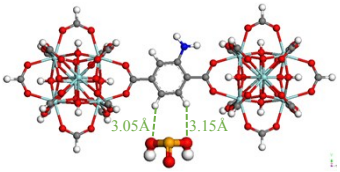  benzene-H—OH-Se(OH)=O | -7496.09 | -8.43 | 3.05/3.15 |
| | | E | 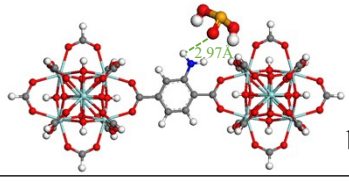  benzene-N(H)-H—O(H)-Se(OH)=O | -7496.09 | -14.99 | 2.97 |
| $SeO_4^{2-}$ | -673.00 | A | 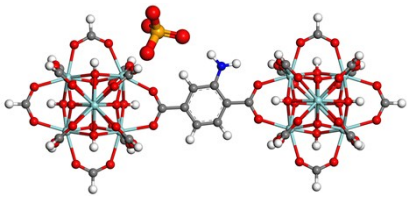 | -7570.39 | -62.07 | 2.21 |

80

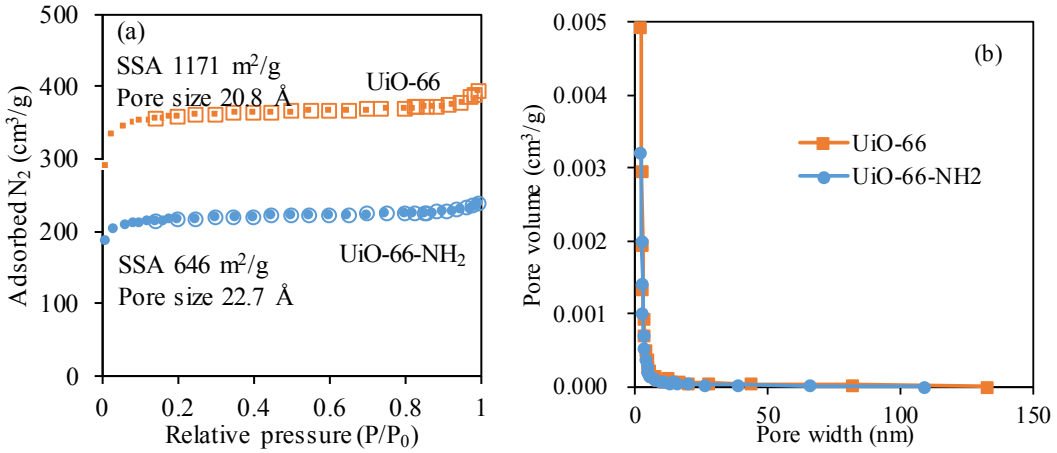


**Fig. S1** $N_2$ adsorption-desorption isotherm plot (a) and BJH pore size distribution (b) of UiO-66 and UiO-66-$NH_2$.

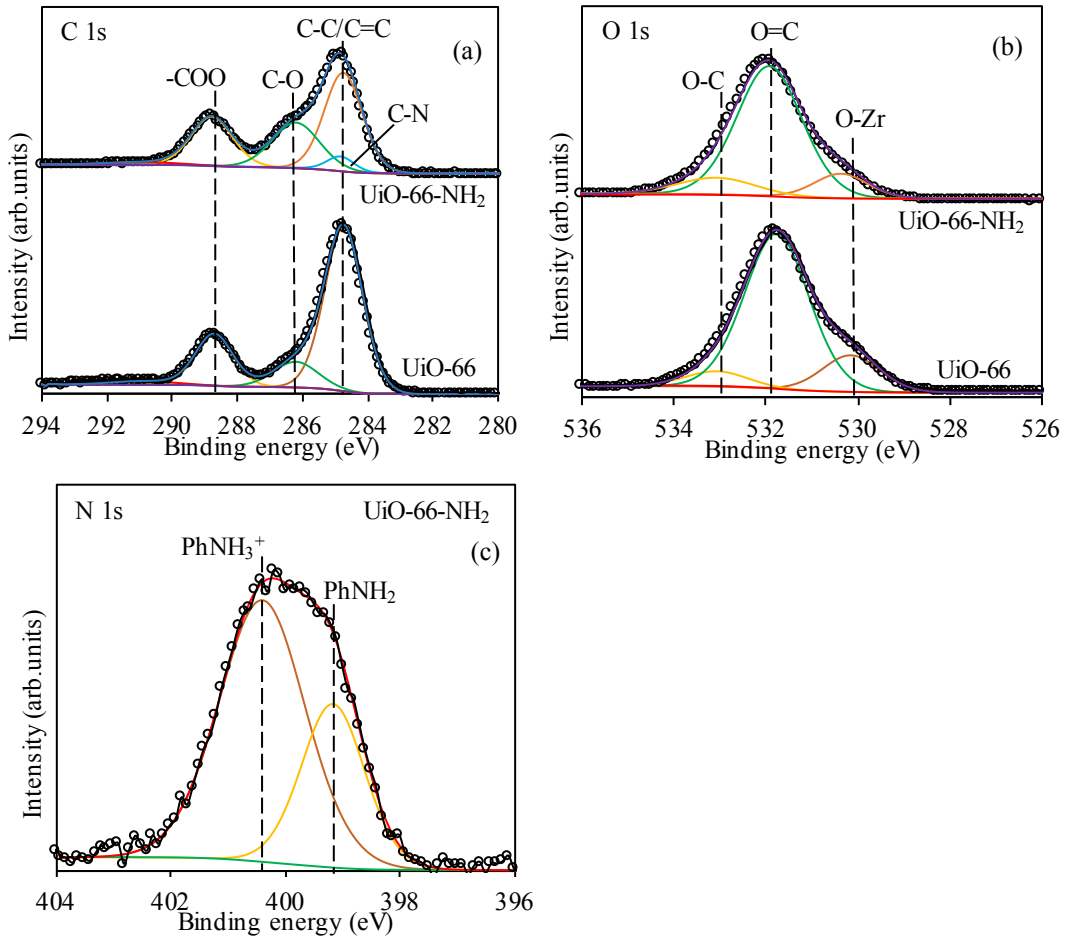


**Fig. S2** C 1s (a), O 1s (b) XPS spectra of UiO-66 and UiO-66-$NH_2$ and N1s (c) XPS spectra of UiO-66-$NH_2$.

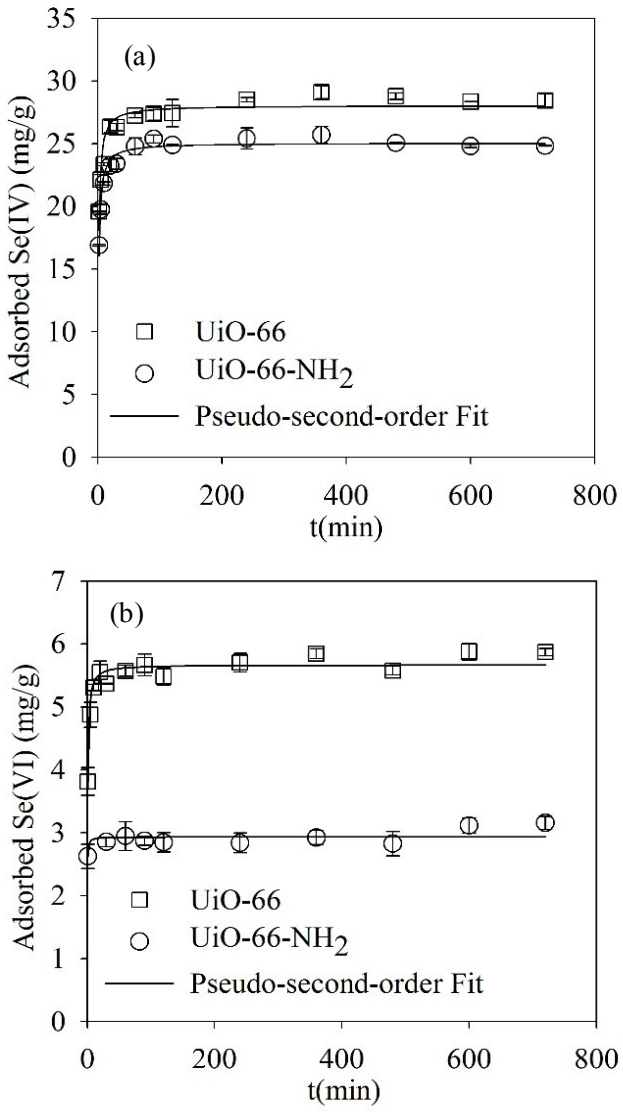


**Fig. S3** Adsorption kinetics of Se(IV) (a) and Se(VI) (b) to UiO-66 and UiO-66-$NH_2$.

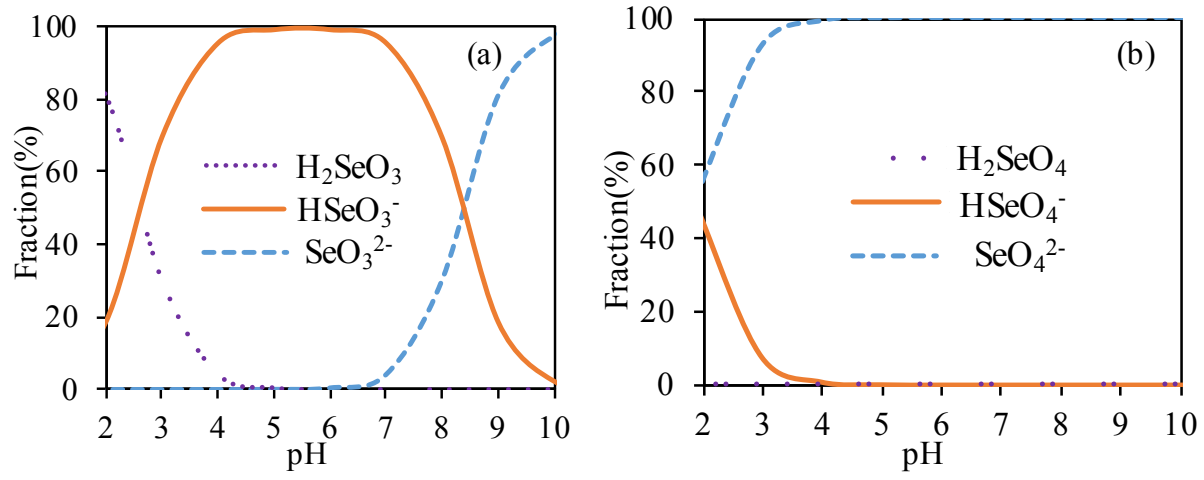

**Fig. S4** Species distribution of (a) Se(IV) and (b) Se(VI) as a function of pH.

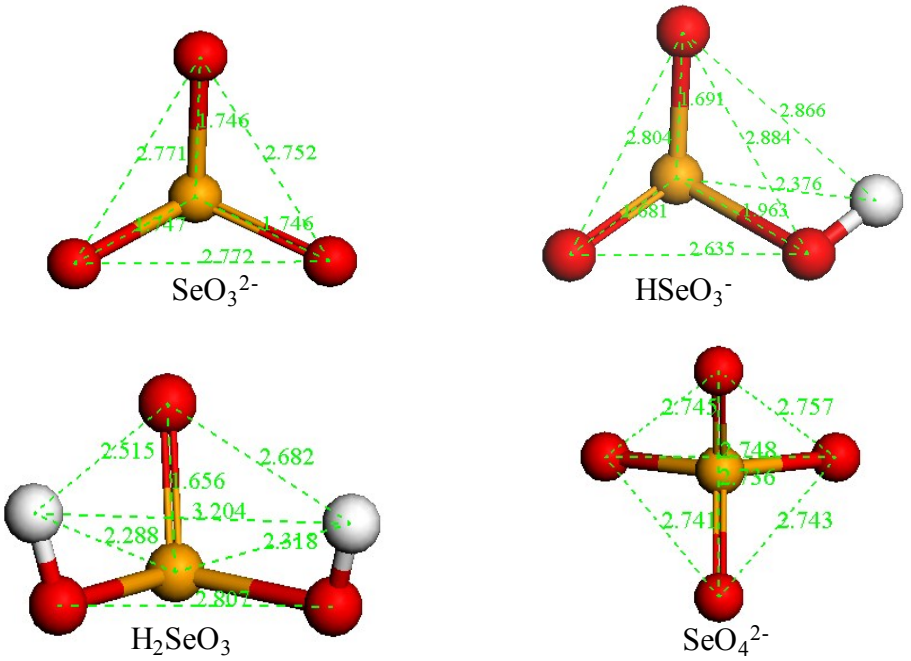


**Fig. S5** Optimized geometry patterns of $SeO_3^{2-}$, $HSeO_3^{-}$, $H_2SeO_3$, and $SeO_4^{2-}$.

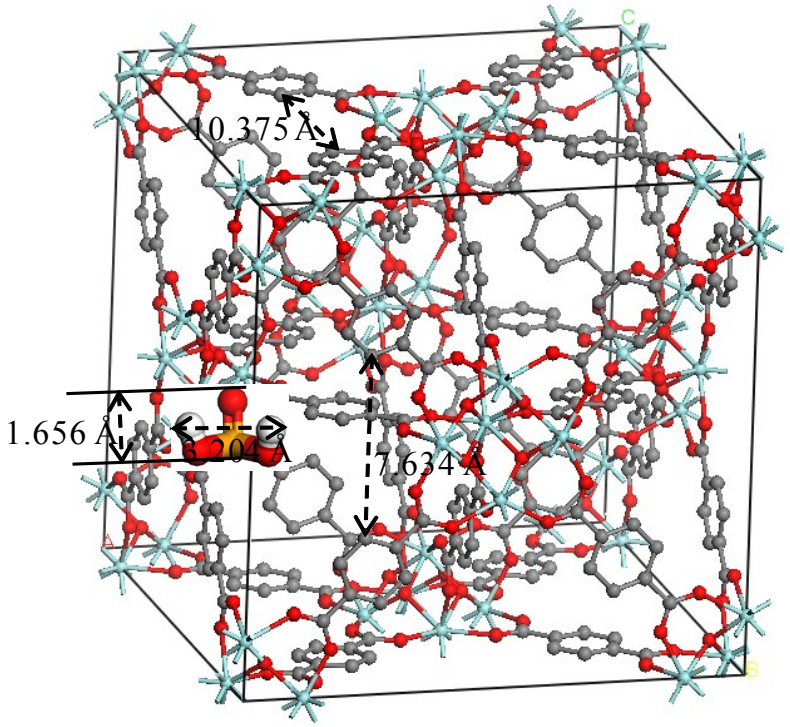


**Fig. S6** Size of $H_2SeO_3$ molecule compared to the distances of the hole of UiO-66.

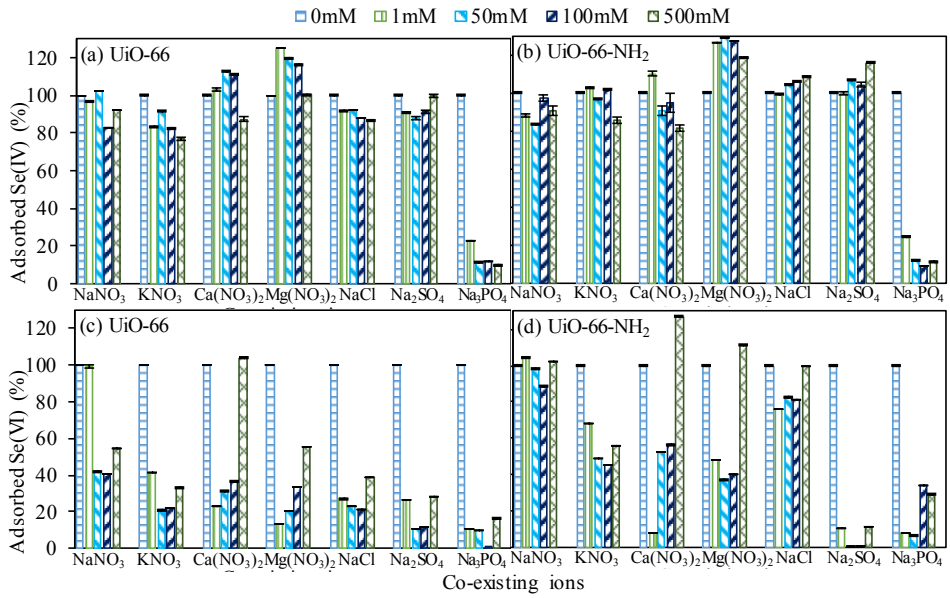


**Fig. S7** Effect of coexisting ions on the adsorption of Se(IV) (a and b) and Se(VI) (c and d) to UiO-66 and UiO-66-$NH_2$.

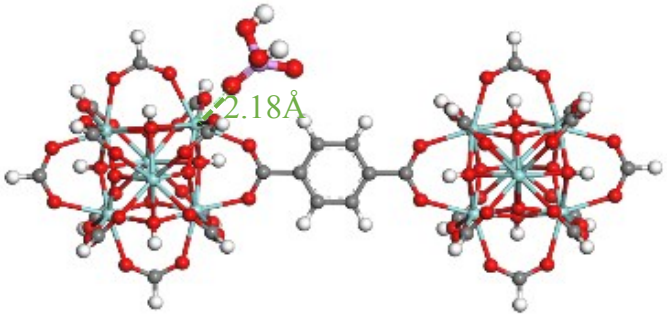


**Fig. S8** Molecular structure for $H_2PO_4^-$ adsorbed on UiO-66.

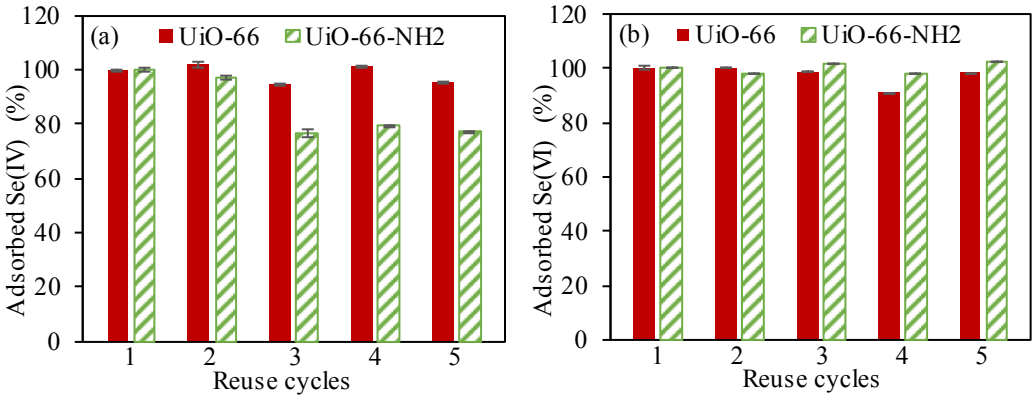


**Fig. S9** Removal of Se(IV) (a) and Se(VI) (b) by the UiO-66/UiO-66-$NH_2$ after regeneration.

## Notes and References


1 J. Ren, H. W. Langmi, B. C. North, M. Mathe and D. Bessarabov, Modulated synthesis of zirconium-metal organic framework (Zr-MOF) for hydrogen storage applications, *Int. J. Hydrogen Energ.*, 2014, **39**, 890-895.

2 S. J. Garibay and S. M. Cohen, Isoreticular synthesis and modification of frameworks with the UiO-66 topology, *Chem. Commun.*, 2010, **46**, 7700-7702.

3 C. Wu, Adsorption of reactive dye onto carbon nanotubes: equilibrium, kinetics and thermodynamics, *J. Hazard. Mater.*, 2007, **144**, 93-100.

4 S. Lagergren, About the theory of so-called adsorption of soluble substances, *Handl.*, 1898, **24**, 1-39.

5 Y. S. Ho, D. J. Wase and C. F. Forster, Kinetic studies of competitive heavy metal adsorption by sphagnum moss peat, *Environ. Technol.*, 1996, **17**, 71-77.

6 Y. Ho and G. McKay, The kinetics of sorption of divalent metal ions onto sphagnum moss peat, *Water Res.*, 2000, **34**, 735-742.

7 W. J. Weber and J. C. Morris, Kinetics of adsorption on carbon from solution, *J. Sanit. Eng. Div. Am. Soc. Civ. Eng.*, 1963, **89**, 31-60.

8 S. Senthilkumaar, P. Kalaamani, K. Porkodi, P. R. Varadarajan and C. V. Subburaam, Adsorption of dissolved reactive red dye from aqueous phase onto activated carbon prepared from agricultural waste, *Bioresource Technol.* 2006, **97**, 1618-1625.

9 W. Sun, W. Pan, F. Wang and N. Xu, Removal of Se(IV) and Se(VI) by $MFe_2O_4$ nanoparticles

from aqueous solution, *Chem. Eng. J.*, 2015, **273**, 353-362.

10 X. Wu, B. Xiao, R. Li, C. Wang, J. Huang and Z. Wang, Mechanisms and factors affecting sorption of microcystins onto natural sediments, *Environ. Sci. Technol.*, 2011, **45**, 2641-2647.

11 W. Sun, J. E. Renew, W. Zhang, Y. Tang and C. Huang, Sorption of Se(IV) and Se(VI) to coal fly ash/cement composite: Effect of $Ca^{2+}$ and high ionic strength, *Chem. Geol.*, 2017, **464**, 76-83.

12 C. M. Gonzalez, J. Hernandez, J. G. Parsons and J. L. Gardea-Torresdey, A study of the removal of selenite and selenate from aqueous solutions using a magnetic iron/manganese oxide nanomaterial and ICP-MS, *Microchem. J.*, 2010, **96**, 324-329.

13 Y. Fu, J. Wang, Q. Liu and H. Zeng, Water-dispersible magnetic nanoparticle-graphene oxide composites for selenium removal, *Carbon*, 2014, **77**, 710-721.

14 J. S. Yamani, A. W. Lounsbury and J. B. Zimmerman, Adsorption of selenite and selenate by nanocrystalline aluminum oxide, neat and impregnated in chitosan beads, *Water Res.*, 2014, **50**, 373-381.

15 L. D. Mafu, T. Msagati and B. B. Mamba, Adsorption studies for the simultaneous removal of arsenic and selenium using naturally prepared adsorbent materials, *Int. J. Environ. Sci. Te.*, 2014, **11**, 1723-1732.

16 N. Bleiman and Y. G. Mishael, Selenium removal from drinking water by adsorption to chitosan-clay composites and oxides: batch and columns tests, *J. Hazard. Mater.*, 2010, **183**, 590-595.

147 17 M. R. Awual, M. M. Hasan and M. A. Khaleque, Efficient selenium(IV) detection and
148 removal from water by tailor-made novel conjugate adsorbent, *Sensor. Actuat. B: Chem.*, 2015,
149 **209**, 194-202.
150 18 M. R. Awual, T. Yaita, S. Suzuki and H. Shiwaku, Ultimate selenium(IV) monitoring and
151 removal from water using a new class of organic ligand based composite adsorbent, *J. Hazard.*
152 *Mater.*, 2015, **291**, 111-119.
153 19 M. R. Awual, M. M. Hasan, T. Ihara and T. Yaita, Mesoporous silica based novel conjugate
154 adsorbent for efficient selenium(IV) detection and removal from water, *Micropor. Mesopor.*
155 *Mat.*, 2014, **197**, 331-338.
156 20 X. Wei, S. Bhojappa, L. Lin and R. C. Viadero Jr, Performance of nano-magnetite for removal
157 of selenium from aqueous solutions, *Environ. Eng. Sci.*, 2012, **29**, 526-532.
158 21 C. M. Gonzalez, J. Hernandez, J. R. Peralta-Videa, C. E. Botez, J. G. Parsons and J. L. Gardea-
159 Torresdey, Sorption kinetic study of selenite and selenate onto a high and low pressure aged
160 iron oxide nanomaterial, *J. Hazard. Mater.*, 2012, **211**, 138-145.
161 22 J. Fu, X. Zhang, S. Qian and L. Zhang, Preconcentration and speciation of ultra-trace Se(IV)
162 and Se(VI) in environmental water samples with nano-sized $TiO_2$ colloid and determination by
163 HG-AFS, *Talanta*, 2012, 94, 167-171.
164 23 N. Chubar, EXAFS and FTIR studies of selenite and selenate sorption by alkoxide-free sol-
165 gel generated Mg-Al-$CO_3$ layered double hydroxide with very labile interlayer anions, *J. Mater.*
166 *Chem. A*, 2014, **2**, 15995-16007.

24 J. Das, B. S. Patra, N. Baliarsingh and K. M. Parida, Calcined Mg-Fe-$CO_3$ LDH as an adsorbent for the removal of selenite, *J. Colloid Interf. Sci.*, 2007, **316**, 216-223.

25 A. W. Lounsbury, J. S. Yamani, C. P. Johnston, P. Larese-Casanova and J. B. Zimmerman, The role of counter ions in nano-hematite synthesis: Implications for surface area and selenium adsorption capacity, *J. Hazard. Mater.*, 2016, **310**, 117-124.

26 M. Szlachta and N. Chubar, The application of Fe-Mn hydrous oxides based adsorbent for removing selenium species from water, *Chem. Eng. J.*, 2013, **217**, 159-168.

27 L. Zhang, N. Liu, L. Yang and Q. Lin, Sorption behavior of nano-$TiO_2$ for the removal of selenium ions from aqueous solution, *J. Hazard. Mater.*, 2009, **170**, 1197-1203.

28 A. J. Howarth, M. J. Katz, T. C. Wang, A. E. Platero-Prats, K. W. Chapman, J. T. Hupp and O. K. Farha, High Efficiency adsorption and removal of selenate and selenite from water using metal-organic frameworks, *J. Am. Chem. Soc.*, 2015, **137**, 7488-7494.

29 J. Li, Y. Liu, X. Wang, G. Zhao, Y. Ai, B. Han, T. Wen, T. Hayat, A. Alsaedi and X. Wang, Experimental and theoretical study on selenate uptake to zirconium metal-organic frameworks: Effect of defects and ligands, *Chem. Eng. J.*, 2017, **330**, 1012-1021.

30 J. Lessa, A. M. Araujo, G. Silva, L. Guilherme and G. Lopes, Adsorption-desorption reactions of selenium(VI) in tropical cultivated and uncultivated soils under Cerrado biome, *Chemosphere*, 2016, **164**, 271-277.